J. Chem. Sci. Vol. 129, No. 7, July 2017, pp. 1061–1067. © Indian Academy of Sciences.
DOI 10.1007/s12039-017-1281-7

REGULAR ARTICLE

Special Issue on THEORETICAL CHEMISTRY/CHEMICAL DYNAMICS

The dynamic behavior of the exohedral transition metal complexes of B_{40} : η^6- and η^7-$B_{40}Cr(CO)_3$ and $Cr(CO)_3$-η^7-B_{40} -η^7-$Cr(CO)_3$†

NAIWRIT KARMODAK and ELUVATHINGAL D JEMMIS*
Department of Inorganic and Physical Chemistry, Indian Institute of Science, Bangalore, Karnataka 560 012, India
E-mail: jemmis@ipc.iisc.ernet.in

MS received 16 February 2017; accepted 13 April 2017

Abstract. The dynamic nature of the exohedral η^6- and the η^7-complexes of B_{40} with $Cr(CO)_3$ has been explored using density functional theory. The *ab initio* molecular dynamic simulations were performed at 1200 K to investigate the fluxionality of the heptagonal and hexagonal faces of exohedral B_{40} complexes. Our computations show that the coordination of the B_{40} faces with $Cr(CO)_3$ fragment reduces its fluxionality to a limited extent. The activation barrier for the inter-conversion of the heptagonal and hexagonal rings in $(CO)_3Cr(\eta^6\text{-}B_{40})$ complex is around 15.2 kcal/mol whereas in the $(CO)_3Cr(\eta^7\text{-}B_{40})$ complex, it is slightly higher at around 19.7 kcal/mol. The coordination with another $Cr(CO)_3$ fragment is found to be equally exergonic, with a barrier for interconversion of 21.5 kcal/mol. The HOMO-LUMO gap is almost similar as the mono-metallated complexes. The di-metallated complexes also show a dynamical behavior of the six and seven membered rings at 1200 K.

Keywords. Borospherenes; Density functional theory; Half-sandwich complexes; Fluxionality; Molecular dynamics.

1. Introduction

The chemistry of fullerenes have been a major success story of spheroidal molecules during the last 30 years. The classical five and six membered rings with 2c-2e bonds rendered them with robust and rigid structures.[1] The skeletal rearrangements and fragmentation of fullerenes required extreme conditions.[2–4] Until recently, attempts to generate similar spheroidal boron analogs met with failure.[5] Computational studies of boron clusters and the nature of polyhedral boranes suggested that the surface of borospherenes may be constituted by triangular network.

Recent characterization of B_{40} has given an added impetus to the study of borospherenes.[6–11] Though the structure of B_{40} is approximately spherical (Figure 1a) with 48 three membered rings, it has 2 six membered rings juxtaposed to each other and 4 seven membered rings. The Schlegel diagram in Figure 1b and 1c show the arrangement of the triangular rings along with the position of the hexagonal and heptagonal rings in B_{40}. There has been several studies on the electronic structure and stability of borospherenes.[5–11] The inevitability of larger rings (holes) in borospherenes and borophenes have been demonstrated.[12–17] It is possible to "close" the larger holes by complexation to transition metal fragments. Does this make the skeleton more rigid?[16] It is tempting to generalize that the multicenter nature of the bonding predisposes borospherenes to dynamic reorganizations, while the classical localized 2c-2e σ-bonds keep the carbon fullerene rigid. However, this is not the complete story. The hydrocarbons such as bullvalene and semi-bullvalene show unusual fluxionality despite "localized" C-C bonds,[19–21] whereas delocalized bonding in $B_{12}H_{12}^{-2}$ only strengthens the boron skeleton.[22] The borospherenes considered here are indeed floppy molecules.[18,23]

Computational studies of Guajardo *et al.,* on B_{40} have shown that though the caged structure is maintained, the heptagonal and hexagonal rings are interconvertible to each other with a very low energy barrier of 14.3 kcal/mol.[18] The positional displacement of the boron atoms constituting the hexagonal and heptagonal rings leads to the fluxional behavior of this boron cage. The Figure 2 shows the initial (**I**), Transition state (TS, **II**) and one of the intermediate (**III**) geometries of B_{40} depicting the structural changes associated during the interconversion of the seven and six membered

*For correspondence

†Dedicated to the memory of the late Professor Charusita Chakravarty.

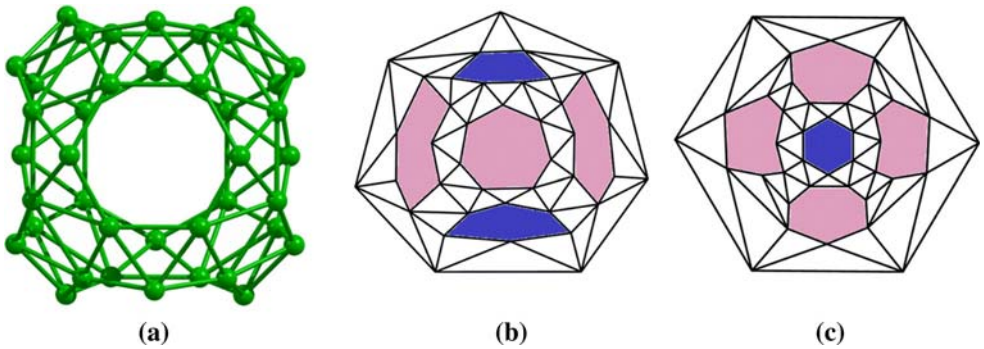

Figure 1. **a** The molecular structure of B_{40}. **b**, **c** Represent the Schlegel diagram of B_{40} through the heptagonal and hexagonal faces.

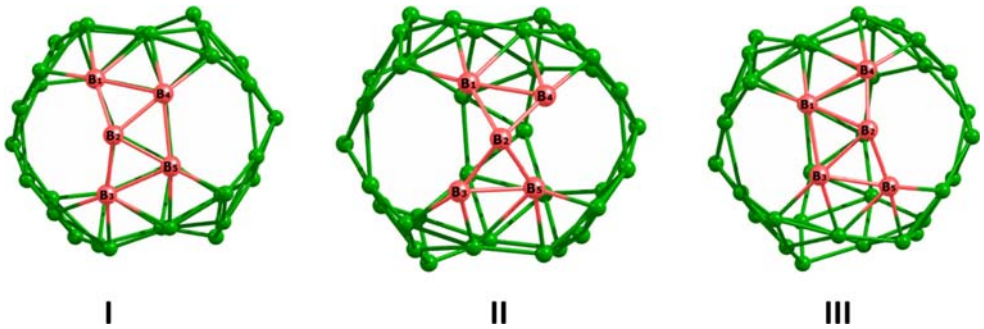

Figure 2. The structural changes in geometry observed by Guajardo *et al.*,[18] while simulating at 1200 K. (I) Initial geometry; (II) transition state; (III) the intermediate geometry obtained after interconversion of the six and the seven membered rings. Rearrangement of the boron atoms B1–B5 shown as pink spheres results in interconversion of the six to seven membered rings.

rings. The boron atom, B_2 moves from the B7 ring towards the adjacent B6 ring. This reduces the distance between B_1 and B_3, whereas the B_4–B_5 bond distance is increased. Thus giving rise to the interconversion of the six and seven membered rings. The presence of multicenter bonding pattern is considered to be the mediating factor for this intercoversion.[5,18] The aromaticity of the cage also remains conserved during the conversion.

Several strategies were examined computationally to enhance the stability of B_{40} fullerene, by complexation with alkali, alkaline and transition metals exohedrally and endohedrally.[24–28] We had shown that the aromaticity and stability of B_{40} increase by exohedral complexation with transition metal-arene fragments such as $Cr(C_6H_6)$, $Cr(CO)_3$, $Mn(C_5H_5)$, $Fe(C_4H_4)$ and $Co(C_3H_3)$ through the hexagonal and heptagonal rings.[16] The $Pd(PH_3)_2$ and $Pt(PH_3)_2$ fragments could effectively bind with the triangular units of B_{40}. It is expected that closing the holes in B_{40} by complexation may impart greater mechanical stability to the skeleton and reduce the fluxionality. Here, we investigate the dynamical behavior of the η^7- and η^6- exohedral complexes of B_{40} with $Cr(CO)_3$ fragment and compare the results with the parent system using *ab initio* molecular dynamic simulations (AIMD) at finite temperature.

2. Computational details

The exohedral complexes of B_{40} with $Cr(CO)_3$ fragments were optimized at PBE0/Def2-SVP[29–32] using Gaussian 09 package.[33] Frequencies were calculated at the same level of theory. The Nucleus-independent chemical shift (NICS) values of the complexes were computed using gauge-independent atomic orbital method.[34] The *ab initio* dynamic simulations were done using PBE[35] functional and plane wave basis set with Vienna *ab initio* simulation package (VASP).[36–39] PAW pseudopotentials were used to treat the electron ion interactions.[37] The energy cutoff for the plane wave basis set was 400 eV and the k points were set to gamma points only for all computations. The electronic energy convergence threshold was set to 10^{-6} eV for energy and 10^{-3} eV/Å for force. The *ab initio* molecular dynamic simulations were performed for 16 ps with canonical (NVT) ensemble using the algorithm of Nose[40] at finite temperature of 1200 K with a time step of 1.0 fs (since B_{40} was found to show dynamical behavior at this temperature).[18] The initial

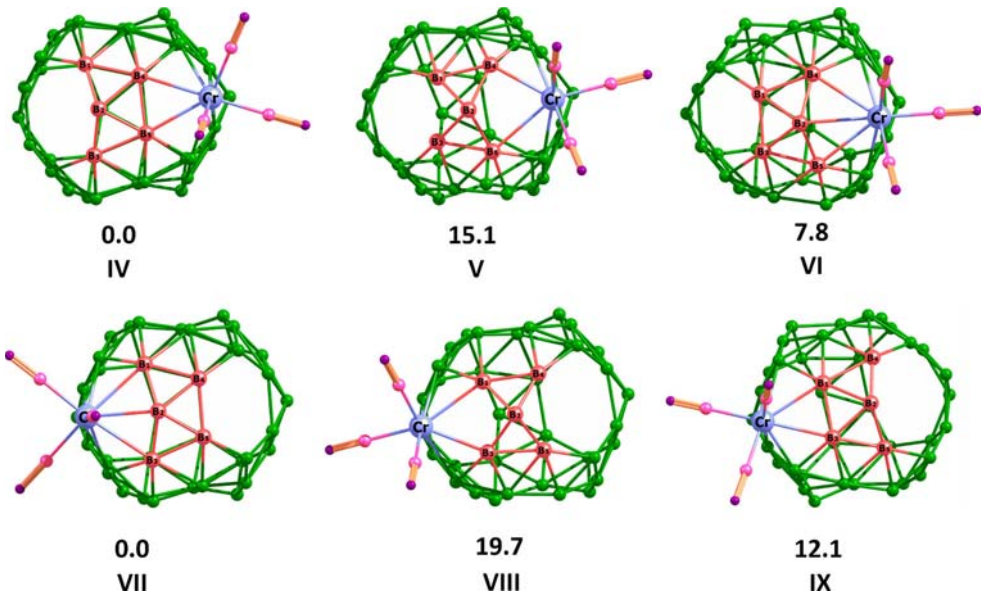

Figure 3. The structural changes in the η^6- and η^7-exohedral complexes of B_{40} with $Cr(CO)_3$ fragment. The zero-point corrected relative energy values in kcal/mol are mentioned. **(IV)–(VI)** denote the initial, TS and the final geometries for η^6-exohedral complex. **(VII)–(IX)** denote the initial, TS and the final geometries for η^7-exohedral complex. The rearrangement of boron atoms in the B_{40} cage leading to the interconversion of six and seven membered rings are denoted as B_1 to B_5.

structures were built up from the corresponding optimized molecular structures obtained from Gaussian output.

3. Results and Discussion

The diagrammatic representation of the initial, TS and the intermediate geometries of the exohedral η^6- and η^7-B_{40} complexes with $Cr(CO)_3$ fragment, observed during the dynamic simulations at 1200 K are shown in Figure 3. Zero-point energy corrected relative energies in kcal/mol are also given here. The *ab initio* dynamic simulations of the two complexes show a behavior similar to that of B_{40}. Interconversion of the heptagonal and hexagonal rings for both the exohedral complexes at 1200 K are shown in the movie SM1 and SM2 (supplementary information). The interconversion follows a similar pathway, where one of the boron atoms (B_2 in Figure 3) of the heptagonal rings interchange its position with a boron of a three membered ring. In our calculations, the interconversion between the heptagonal and hexagonal rings for both the complexes are observed after 12 ps from the initial time period. The detailed transformation pathway and the involved energetics are investigated using Gaussian package. The TS geometries have similarity with that of TS geometry seen for un-complexed B_{40} (Figure 2). In $(CO)_3Cr(\eta^6\text{-}B_{40})$ (**IV**) after rearrangement of the hexagonal and heptagonal rings, the relative energy of the intermediate structure increases by 7.8 kcal/mol. In this geometry (**VI**), the two hexagonal rings acquire an adjacent position within the cage, unlike the starting geometry where the two hexagonal rings are present opposite to each other. The TS in this case is found to be around 15.1 kcal/mol higher in energy with respect to the starting geometry (**IV**). In the η^7-exohedral complex (**VII**), the relative energy of the intermediate structure (**IX**) w.r.t. the initial structure is around 12.1 kcal/mol. The rearrangement of the boron atoms in the transition state geometry (**VIII**) connecting **VII** and **IX** is similar to the transition state structures obtained for $(CO)_3Cr(\eta^6\text{-}B_{40})$ complex and the un-complexed B_{40}. The activation barrier is around 19.1 kcal/mol, slightly higher than that observed for η^6-complex. In order to correlate the barrier heights for interconversion of the B6 and B7 rings in the two exohedral complexes to that of the un-complexed B_{40}, we have recalculated the optimized energies of the initial, TS and the intermediate geometries for B_{40} as shown in Figure 2, using similar functionals and basis sets. The activation barrier in this case is found to be around 15.2 kcal/mol, whereas the intermediate geometry (Figure 2c) is around 11.5 kcal/mol higher than that of the initial structure (**I**). These relative energy values are in close resemblance to the previous report (activation barrier is reported to around 14.8‘kcal/mol and relative energy of the final geometry is computed to around 11.2 kcal/mol w.r.t. the initial structure).[18] The activation barrier for the η^6-

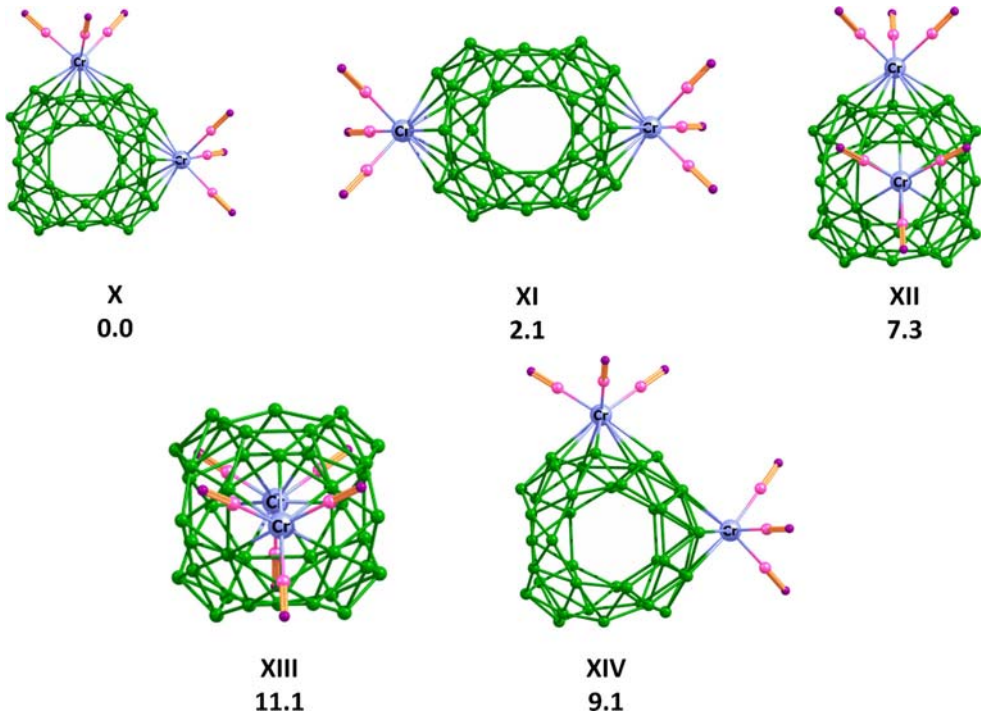

Figure 4. The exohedral B_{40} complexes with two $Cr(CO)_3$ fragments. (X) Two adjacent B7 rings of B_{40} are coordinated. (XI) The two B7 rings oriented opposite to each other are coordinated. (XII) One of the B7 and B6 rings are bound to the metal-ligand fragment. (XIII) The two hexagonal rings are coordinated. (XIV) The final structure formed from **3a** during simulation, where one of the heptagonal ring is transformed to the hexagonal ring. The relative energy values in kcal/mol are given.

complex is almost equivalent to the un-complexed B_{40}. However, for the η^7-complex, the activation barrier for interconversion increases slightly. This trend is anticipated due to the better overlap between the B7 ring of $B_{40}$with $Cr(CO)_3$ fragment, in comparison to the η^6-complex.[16] The relative differences in energy between the intermediate (**IX**) and the initial (**VII**) geometries for the η^7-complex is nearly similar to the un-complexed B_{40}, whereas in η^6-complex the corresponding relative energy difference is reduced as shown in Figure 3.

Since exohedral complexation with a single $Cr(CO)_3$ fragment brings in only marginal changes in the dynamical behavior, we have further studied the dynamical behavior of B_{40} coordinated to two $Cr(CO)_3$ fragments (Figure 4, **X-XIII**). The attachment of another $Cr(CO)_3$ fragment to $(CO)_3Cr(\eta^7\text{-}B_{40})$ would result in three isomers and $(CO)_3Cr(\eta^6\text{-}B_{40})$ would provide two isomers. However, one of the isomers from $(CO)_3Cr(\eta^6\text{-}B_{40})$ is same as the one isomer obtained from $(CO)_3Cr(\eta^7\text{-}B_{40})$. Thus, total four non-equivalent possibilities are obtained for the exohedral complexes with two $Cr(CO)_3$ fragments as shown in Figure 4. Table 1 reports the HOMO-LUMO gaps and the NICS values at the approximate centroid for all the isomers. The relative energy differences between the isomers are very less as seen earlier for the mono-metallated η^6- and η^7-complexes of B_{40}.[16] The two complexes (**X** and **XI**), where two adjacent or the opposite heptagonal faces of B_{40} are coordinated to the $Cr(CO)_3$ fragments have the highest stability.

$$B_{40} + (CO)_3Cr(\eta^6\text{-}C_6H_6) \rightarrow (CO)_3Cr(\eta^n\text{-}B_{40}) + C_6H_6$$
$$\Delta H: -23.5 \text{ kcal/mol, n} = 7 \quad (\mathbf{IV})$$
$$-20.5 \text{ kcal/mol, n} = 6 \quad (\mathbf{VII}) \qquad (1)$$

$$(CO)_3Cr(\eta^7\text{-}B_{40}) + (CO)_3Cr(\eta^6\text{-}C_6H_6)$$
$$\rightarrow (CO)_3Cr(\eta^7\text{-}B_{40}\text{-}\eta^7)Cr(CO)_3 + C_6H_6$$
$$\Delta H: -23.3 \text{ kcal/mol}, \quad \text{for } \mathbf{X}$$
$$-21.3 \text{ kcal/mol}, \quad \text{for } \mathbf{XI} \qquad (2)$$

$$(CO)_3Cr(\eta^6\text{-}B_{40}) + (CO)_3Cr(\eta^6\text{-}C_6H_6)$$
$$\rightarrow (CO)_3Cr(\eta^6\text{-}B_{40}\text{-}\eta^7)Cr(CO)_3 + C_6H_6$$
$$\Delta H: -19.5 \text{ kcal/mol}, \quad \text{for } \mathbf{XII} \qquad (3)$$

$$(CO)_3Cr(\eta^6\text{-}B_{40}) + (CO)_3Cr(\eta^6\text{-}C_6H_6)$$
$$\rightarrow (CO)_3Cr(\eta^6\text{-}B_{40}\text{-}\eta^6)Cr(CO)_3 + C_6H_6$$
$$\Delta H: -15.7 \text{ kcal/mol}, \quad \text{for } \mathbf{XIII} \qquad (4)$$

The other two isomers where the adjacent hexagonal and heptagonal faces or both the hexagonal faces (complex XI and XII) coordinate to $Cr(CO)_3$ fragments are

Table 1. The HOMO-LUMO gap (in eV) and the NICS values (in ppm) at the center of the B40 complexes calculated at PBE0/Def2-SVP using Gaussian g09 package.[29–33]

Complex	HOMO-LUMO gap (eV)	NICS at the center (ppm)
B_{40}(**I**)	3.1	−41.6
$(CO)_3Cr(\eta^6\text{-}B_{40})$ (**IV**)	2.9	−49.1
$(CO)_3Cr(\eta^7\text{-}B_{40})$ (**VI**)	2.6	−48.1
$(CO)_3Cr(\eta^7\text{-}B_{40})$ (**VII**)	2.6	−44.9
$(CO)_3Cr(\eta^6\text{-}B_{40})$ (**IX**)	2.5	−48.2
$(CO)_3Cr(\eta^7\text{-}B_{40}\text{-}\eta^7)Cr(CO)_3$(**X**)	2.6	−49.4
$(CO)_3Cr(\eta^7\text{-}B_{40}\text{-}\eta^7)Cr(CO)_3$(**XI**)	2.5	−44.5
$(CO)_3Cr(\eta^7\text{-}B_{40}\text{-}\eta^6)Cr(CO)_3$(**XII**)	2.6	−52.6
$(CO)_3Cr(\eta^6\text{-}B_{40}\text{-}\eta^6)Cr(CO)_{3\_}$(**XIII**)	2.6	−48.3
$(CO)_3Cr(\eta^7\text{-}B_{40}\text{-}\eta^6)Cr(CO)_3$(**XIV**)	2.4	−49.2

The HOMO-LUMO gaps calculated for $C_{60}Pd(PH_3)_2$ and $C_{60}Pt(PH_3)_2$ at the same level of theory and basis set are around 2.7 and 2.6 eV, respectively.

less stable by 7.34 and 11.12 kcal/mol than complex X respectively. This is due to the better overlap between the seven membered rings of B_{40} with $Cr(CO)_3$ fragment compared to the B6 rings.

Near-isodesmic equations (eqs. 1–4) show that the coordination of second $Cr(CO)_3$ fragment to the $(CO)_3Cr(\eta^7\text{-}B_{40})$ and $(CO)_3Cr(\eta^6\text{-}B_{40})$ is equally exergonic as the coordination of one $Cr(CO)_3$ fragment with B6 or B7 ring of B_{40}. The attachment of one $Cr(CO)_3$ fragment to the heptagonal or hexagonal face is exothermic by about 23.5 and 20.5 kcal/mol (eq. 1) respectively. The exothermicity of the near-isodesmic equation for coordination of another $Cr(CO)_3$ fragment ranges between 23.3 to 15.7 kcal/mol as shown in eqs. 2 and 3. The HOMO-LUMO separations for the four isomers are also almost equivalent to the $(CO)_3Cr(\eta^6\text{-}B_{40})$ and $(CO)_3Cr(\eta^7\text{-}B_{40})$ complexes and the C_{60} complexes with $Pd(PH_3)_2$ and $Pt(PH_3)_2$ fragment (Table 1). The negative NICS values for all the isomers at the center of the cage shows the presence of aromatic ring current. These NICS values vary from −49.4 ppm in **X** to −48.3 ppm in **XIII**. In order to investigate the dynamical behavior of these B_{40} complexes with two $Cr(CO)_3$ fragments, the complex **X** was simulated at 1200 K. The movie SM3 (see Supplementary Information) provides an overview of the dynamic nature of this complex. During the simulation, several intermediate structures were seen. Here, we have calculated the optimized geometry of one such intermediate structure as shown in **XIV**, where one of the heptagonal rings attached with the $Cr(CO)_3$ fragment has converted into a hexagonal ring. The relative energy difference with that of the initial conformation is around 9.4 kcal/mol, calculated at PBE0/Def2-SVP. The NICS value for this intermediate structure is around −49.2, quite similar to the initial structure (**X**). The transition barrier connecting the complex **X** to the intermediate structure **XIV** is calculated to be around 21.5 kcal/mol.

In the exohedral complexes, the B_{40} bonding orbitals are stabilized slightly and the aromatic nature is enhanced as shown in the previous studies.[16] Thus, the delocalized bonding picture of B_{40} remains unaffected after complexation. The fluxionality of the six and the seven membered rings in B_{40} is found to be a consequence of its delocalized bonding picture.[18] Since complexation does not bring drastic changes in the bonding pattern of the B_{40} cage, the dynamic behavior remains largely preserved. However, the extent of overlap between the B_{40} faces and the $Cr(CO)_3$ fragment affects the activation barrier slightly, going from 15.1 to 21.5 kcal/mol. The aromaticity as judged by the NICS values for B_{40} and in various transition metal complexes remains largely invariant. Further complexation with $Cr(CO)_3$ might reduce the fluxional behavior of B_{40}. Thus, we plan to study borospherenes with further complexation to see the effect on their rigidity.

4. Conclusions

The dynamical behavior of the η^6- and η^7- complexes of B_{40} with $Cr(CO)_3$ fragment has been investigated using *ab initio* molecular dynamic simulations. The computations show that coordination of one of the two hexagonal faces of B_{40} with $Cr(CO)_3$ fragment does not affect the activation barrier height for interconversion of the hexagonal ring to the heptagonal ring considerably, in relation to the uncomplexed B_{40}. However, for the exohedral η^7-B_{40} complex, the activation barrier is increased to around 19.7 kcal/mol due to better overlap

of the heptagonal face with the $Cr(CO)_3$ fragment. The dynamic nature of B_{40} remains preserved after coordination of another $Cr(CO)_3$ fragment with the other faces of the exohedral B_{40} complexes. The attachment of another $Cr(CO)_3$ fragment to the η^7-exohedral complex of B_{40} is equally stabililizing. The near-isodesmic equations connecting the mono-metallated η^7-exohedral complex of B_{40} to the dimetallated complexes are exothermic in nature with ΔH varying within the range of -23.3 to -15.7 kcal/mol (the ΔH value for attachment of one $Cr(CO)_3$ fragment to one of the seven membered rings to form η^7-complexes is around -23.5 kcal/mol). The HOMO-LUMO gaps are substantial and comparable to the mono-metallated B_{40} complexes and the fullerene complexes with $Pd(PH_3)_2$ and $Pt(PH_3)_2$ fragments. Thus, these exohedral complexes of B_{40} could be observed experimentally. Since the delocalized bonding picture in B_{40} remains un-altered after complexation, as indicated by the NICS values calculated at the approximate centroid, the dynamic nature of the η^6- and η^7- or the dimetallated B_{40} complexes.

Supplementary Information (SI)

Computational data including cartesian coordinates, variation of root mean square displacements and multimedia files of molecular dynamics (SM1.mp4, SM2.mp4 and SM3.mp4) are provided as the supplementary information, available at www.ias.ac.in/chemsci.

Acknowledgements

The authors are thankful to Inorganic and Physical chemistry department and Supercomputer Education and Research Centre for computational facilities, Council of Scientific and Industrial Research for a Senior Research Fellowship to NK and Department of Science and Technology for the J C Bose fellowship to EDJ.

References

1. Kroto H W, Heath J R, O'Brien S C, Curl R F and Smalley R E 1985 C_{60}: Buckminsterfullerene *Nature* **318** 162
2. Serra S, Sanguinetti S and Colombo L 1994 Pre-fragmentation dynamics of C60. A molecular dynamics investigation *Chem. Phys. Lett.* **225** 191
3. Openov L A and Podlivaev A I 2006 Simulation of the thermal fragmentation of fullerene C_{60} *JETP Lett.* **84** 68
4. L H Green M and H H Stephens A 1997 Fluxional processes in organotransition-metal C_{60} complexes *Chem. Commun.* 793
5. Zhai H-J, Zhao Y-F, Li W-L, Chen Q, Bai H, Hu H-S, Piazza Z A, Tian W-J, Lu H-G, Wu Y-B, Mu Y-W, Wei G-F, Liu Z-P, Li J, Li S-D and Wang L-S 2014 Observation of an all-boron fullerene *Nat. Chem.* **6** 727
6. Chen Q, Li W-L, Zhao Y-F, Zhang S-Y, Hu H-S, Bai H, Li H-R, Tian W-J, Lu H-G, Zhai H-J, Li S-D, Li J and Wang L-S 2015 Experimental and Theoretical Evidence of an Axially Chiral Borospherene *ACS Nano* **9** 754
7. Chen Q, Zhang S-Y, Bai H, Tian W-J, Gao T, Li H-R, Miao C-Q, Mu Y-W, Lu H-G, Zhai H-J and Li S-D 2015 Cage-Like B_{41}^+ and B_{42}^{2+}: New Chiral Members of the Borospherene Family *Angew. Chem., Int. Ed.* **54** 8160
8. Lv J, Wang Y, Zhu L and Ma Y 2014 B_{38}: an all-boron fullerene analogue *Nanoscale* **6** 11692
9. Tai T B and Nguyen M T 2016 A new chiral boron cluster B44 containing nonagonal holes *Chem. Commun.* **52** 1653
10. Zhao J, Huang X, Shi R, Liu H, Su Y and King R B 2015 B28: The smallest all-boron cage from an ab initio global search *Nanoscale* **7** 15086
11. Li H-R, Jian T, Li W-L, Miao C-Q, Wang Y-J, Chen Q, Luo X-M, Wang K, Zhai H-J, Li S-D and Wang L-S 2016 Competition between quasi-planar and cage-like structures in the B_{29}^- cluster: Photoelectron spectroscopy and ab initio calculations *Phys. Chem. Chem. Phys.* **18** 29147
12. Tang H and Ismail-Beigi S 2007 Novel Precursors for Boron Nanotubes: The Competition of Two-Center and Three-Center Bonding in Boron Sheets *Phys. Rev. Lett.* **99** 115501
13. Wu X, Dai J, Zhao Y, Zhuo Z, Yang J and Zeng X C 2012 Two-Dimensional Boron Monolayer Sheets *ACS Nano* **6** 7443
14. Galeev T R, Chen Q, Guo J-C, Bai H, Miao C-Q, Lu H-G, Sergeeva A P, Li S-D and Boldyrev A I 2011 Deciphering the mystery of hexagon holes in an all-boron graphene α-sheet *Phys. Chem. Chem. Phys.* **13** 11575
15. Polad S and Ozay M 2013 A new hole density as a stability measure for boron fullerenes *Phys. Chem. Chem. Phys.* **15** 19819
16. Karmodak N and Jemmis E D 2016 Exohedral Complexation of B_{40}, C_{60} and Arenes with Transition Metals: A Comparative DFT Study *Chem. Asian J.* **11** 3350
17. Karmodak N and Jemmis E D 2017 The Role of Holes in Borophenes: An Ab Initio Study of Their Structure and Stability with and without Metal Templates *Angew. Chem., Int. Ed.* doi:10.1002/anie.201610584
18. Martínez-Guajardo G, Luis Cabellos J, Díaz-Celaya A, Pan S, Islas R, Chattaraj P K, Heine T and Merino G 2015 Dynamical behavior of Borospherene: A Nanobubble *Sci. Rep.* **5** 11287
19. von E Doering W and Roth W R 1963 A rapidly reversible degenerate cope rearrangement: Bicyclo[5.1.0]octa-2,5-diene *Tetrahedron* **19** 715
20. Ault A 2001 The Bullvalene Story. The Conception of Bullvalene, a Molecule That Has No Permanent Structure *J. Chem. Educ.* **78** 924
21. Zimmerman H E and Grunewald G L 1966 The Chemistry of Barrelene. III. A Unique Photoisomerization to Semibullvalene *J. Am. Chem. Soc.* **88** 183
22. Sivaev I B, Bregadze V I and Stefan S 2002 Chemistry of closo-Dodecaborate Anion $[B_{12}H_{12}]^2$: A Review *Collect Czech. Chem. Commun.* **67** 679
23. Liu L, Osorio E and Heine T 2016 Understanding the Central Location of a Hexagonal Hole in a B36 Cluster *Chem. Asian J.* **11** 3220

24. Bai H, Chen Q, Zhai H-J and Li S-D 2015 Endohedral and Exohedral Metalloborospherenes: M@B_{40} (M=Ca, Sr) and M&B_{40} (M=Be, Mg) *Angew. Chem., Int. Ed.* **54** 941
25. Dong H, Hou T, Lee S-T and Li Y 2015 New Ti-decorated B_{40} fullerene as a promising hydrogen storage material *Sci. Rep.* **5** 9952
26. Jin P, Hou Q, Tang C and Chen Z 2015 Computational investigation on the endohedral borofullerenes M@B_{40} (M = Sc, Y, La) *Theor. Chem. Acc.* **134** 1
27. Shakerzadeh E, Biglari Z and Tahmasebi E 2016 M@B_{40} (M= Li, Na, K) serving as a potential promising novel NLO nanomaterial *Chem. Phys. Lett.* **654** 76
28. Bai H, Bai B, Zhang L, Huang W, Mu Y-W, Zhai H-J and Li S-D 2016 Lithium-Decorated Borospherene B_{40}: A Promising Hydrogen Storage Medium *Sci. Rep.* **6** 35518
29. Adamo C and Barone V 1999 Toward reliable density functional methods without adjustable parameters: The PBE0 model *J. Chem. Phys.* **110** 6158
30. Weigend F and Ahlrichs R 2005 Balanced basis sets of split valence, triple zeta valence and quadruple zeta valence quality for H to Rn: Design and assessment of accuracy *Phys. Chem. Chem. Phys.* **7** 3297
31. Schäfer A, Horn H and Ahlrichs R 1992 Fully optimized contracted Gaussian basis sets for atoms Li to Kr *J. Chem. Phys.* **97** 2571
32. Schäfer A, Huber C and Ahlrichs R 1994 Fully optimized contracted Gaussian basis sets of triple zeta valence quality for atoms Li to Kr *J. Chem. Phys.* **100** 5829
33. Frisch M J *et al.* 2009 Gaussian 09, Revision **E.01**, Gaussian, Inc., Wallingford CT
34. Wolinski K, Hinton J F and Pulay P 1990 Efficient implementation of the gauge-independent atomic orbital method for NMR chemical shift calculations *J. Am. Chem. Soc.* **112** 8251
35. Perdew J P, Burke K and Ernzerhof M 1996 Generalized Gradient Approximation Made Simple *Phys. Rev. Lett.* **77** 3865
36. Kresse G and Furthmüller J 1996 Efficient iterative schemes for *ab*-initio total-energy calculations using a plane-wave basis set *Phys. Rev. B* **54** 11169
37. Kresse G and Joubert D 1999 From ultrasoft pseudopotentials to the projector augmented-wave method *Phys. Rev. B* **59** 1758
38. Blöchl P E 1994 Projector augmented-wave method *Phys. Rev. B* **50** 17953
39. Kresse G, Furthmüller J and Hafner J 1995 Ab initio Force Constant Approach to Phonon Dispersion Relations of Diamond and Graphite *Europhys. Lett.* **32** 729
40. Nosé S 1984 A unified formulation of the constant temperature molecular dynamics methods *J. Chem. Phys.* **81** 511